Design of CdZnTe & Crystalline Silicon Tandem Junction Solar cells

Chao Zhou, Haejun Chung, Xufeng Wang, and Peter Bermel

***Abstract*—A tandem photovoltaic system consisting of cadmium zinc telluride/crystalline silicon (CZT/c-Si) combines the successful technologies of cadmium telluride and silicon in a single platform and offers the potential efficiencies up to 46% in theory. However, the highest efficiency fabricated CZT/c-Si tandem cell is only 16.8% today. In this paper, we develop a detailed model for single-junction CZT and tandem CZT/c-Si PV cells, that is verified with experimental data. Based on this model, we propose three hypotheses to explain the anomalously low V_{oc} observed in tandem cells: a low-quality tunnel junction, a Schottky barrier and through-thickness shunting path. We then suggest a simple experiment to distinguish these hypotheses. After that, we provide a physics-based analysis of the magnitude of all the loss mechanisms present in the cell, and an experimental strategy to mitigate each one. Ultimately, we predict that the ideal efficiency of CZT/c-Si tandem cell could reach 34.1%, if all these loss mechanisms were mitigated, and the CZT bandgap were adjusted to 1.8 eV, without requiring any improvement in bulk or surface recombination rates.**

***Index Terms*—II-IV material, tandem cell, loss mechanisms**

I. Introduction

RECENT developments in the photovoltaic industry have shown the great commercial promise of two key material platforms: crystalline silicon (c-Si) [1] and cadmium telluride (CdTe) [2]. Heterojunctions made from c-Si have now reached an efficiency of 25.6% at the laboratory scale using rear emitters [3], while commercial manufacturing is at a cost below $0.58 per peak watt [4]. The separate thin film technology of CdTe with a slightly larger bandgap has recently achieved single-crystal world record efficiencies of 21% [2]. Commercial CdTe modules grown by closed-space sublimation have tracked the recent rise in efficiencies, at a cost of $0.39 per peak watt in manufacturing [4]. Clearly, these developments have been quite impressive and driven massive growth in the industry [5]. On the other hand, the ultimate efficiencies of each technology are approaching the fundamental thermodynamic limits first articulated by Shockley and Queisser, which prevent both of these technologies exceeding 31% [6].

Manuscript received XXXX XX, 2015; revised XXXX XX, 20XX. Support was provided by the Department of Energy, under DOE Cooperative Agreement No. DEEE0004946 (PVMI Bay Area PV Consortium), the Semiconductor Research Corporation, under Research Task No. 2110.006 (Network for Photovoltaic Technologies), and the National Science Foundation Award EEC 1454315 - CAREER: Thermophotonics for Efficient Harvesting of Waste Heat as Electricity.

The authors are with the School of Electrical and Computer Engineering, Purdue University, West Lafayette, IN 47906 USA(e-mail: zhou424@purdue.edu; chung110@purdue.edu; wang159@purdue.edu; pbermel@ecn.purdue.edu)

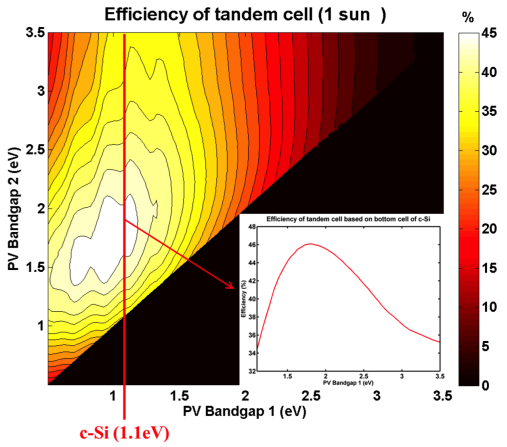

Fig. 1. Theoretical efficiency limit of tandem solar cells as a function of the bandgaps of the bottom cell (PV bandgap 1) and the top cell (PV bandgap 2) [7]. The inset shows the theoretical efficiency limit of tandem cells with a fixed bottom cell (c-Si).

In order for commercial technologies to move substantially above the Shockley-Queisser (S-Q) limit, a fundamentally different approach is needed. While a wide variety of techniques have been discussed [8], the two shown to exceed the S-Q limit experimentally are spectral splitting and multijunctions [9], [10]. The latter approach is conceptually simplest and of great, ongoing interest, since tandem, triple-junction, and 4-junction cells offer theoretical and actual performance substantially higher than the S-Q limit [11].

Broadly speaking, efforts in multijunction cells can be divided into two categories: high-cost, high-performance and low-cost, low-performance cells. In the high-performance category, records have been pushed up over time to a current record of 44.4% for inverted metamorphic 3-junction InGaP/GaAs/InGaAs systems [3]. A similar III-V material platform has also been employed for making world-record efficiency single-junction 28.8% efficient GaAs cells [3]. However, recent estimates have indicated the cost of manufacturing for the single-junction cells even with epitaxial liftoff and significant substrate reuse to be at least $8.45 per peak watt; without any substrate reuse, costs go up above $53 per peak watt [4]. On the low-cost side, 3-junction a-Si/nc-Si/nc-Si cells have reached efficiencies of 13.4% [3]. It is believed that the extremely large gap between these two 3-junction systems is not driven primarily by the value of the bandgaps, which are not very dissimilar, but rather the quality of the materials themselves. In particular, 3-junction thin-film silicon solar cells suffer greatly from the presence of amorphous

silicon [12], which is subject to the Staebler-Wronski effect. Since no other Group IV material offers a similar bandgap, the path to achieving efficiencies comparable to the III-V systems from a crystalline silicon-based platform has been unclear.

Here, we consider an alternative approach for high-performance, low-cost cells that combine the successful technologies of CdTe and c-Si in a single platform. While it may seem almost self-evident to combine these two systems as a tandem cell, the key stumbling block has been the bandgap of cadmium telluride, which is slightly low for this particular application. As shown in Fig. 1, silicon has a bandgap of 1.1 eV, which is close to the ideal bandgap for the bottom junction of a tandem solar cell. However, the ideal bandgap for the top junction is around 1.78 eV. Fortunately, ternary alloys of CdTe offer significantly larger bandgaps, such as CdZnTe [13]–[15], MnCdTe [16] and MgCdTe [17]. In this paper, we focus on CdZnTe (CZT) because of the experimental results available, but the analysis may readily be extended other CdTe ternary alloys. The bandgap of CZT can vary in the range from 1.5 eV [18] up to 2.26 eV [19]. Furthermore, new CdTe and CZT growth techniques such as molecular beam epitaxy offering high crystal quality and bulk lifetimes have been demonstrated [13], [14], [20].

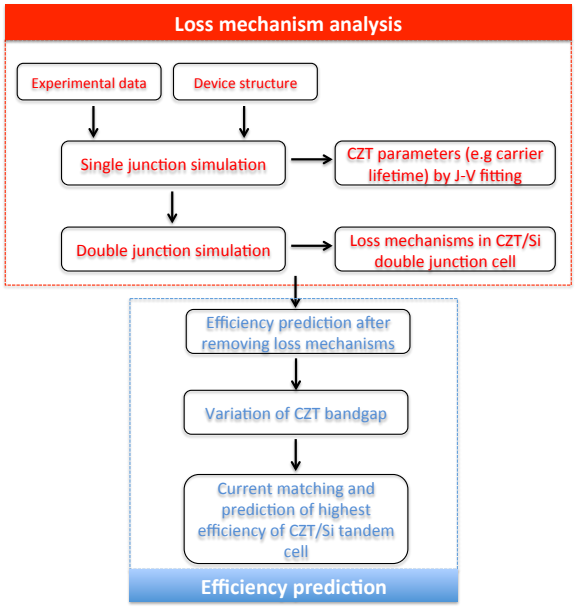

Fig. 2. Structure of this paper. Experimental data and structures are input into our Sentaurus device simulations (detailed in Fig. 3) to accurately predict the performance of single and tandem junction cells in experiment, while quantifying the loss mechanisms. This ultimately allows us to numerically optimize the tandem cells for higher performance.

Using high-quality growth methods, Carmody *et al.* [13], [20] recently fabricated both a CZT single junction solar cell with 16% efficiency and a CZT/c-Si tandem solar cell of 16.8% efficiency – with a surprisingly small 0.8% advantage over the single junction CZT solar cell. We will first develop a detailed understanding of these results with an electro-optical simulation, in which ray tracing will first be used to calculate the light absorption inside the device, and then drift-diffusion will be used to predict the current-voltage relation and recombination losses. Next, we will show that our approach can accurately reproduce experimental observations, including a number of features not found in the Shockley ideal diode equation. In the particular case of the tandem V_{oc} deficit, we will show that there are three potential hypotheses that can be distinguished by a simple experiment. This understanding will then allow us to analyze and explain the key loss mechanisms decreasing the efficiency of the CZT/c-Si tandem solar cell. We will then propose a series of experimental steps that can be taken to mitigate these losses. Finally, we will predict the highest attainable efficiencies for wafer-based CZT/c-Si tandem cells.

This paper is structured as follows (Fig. 2): First, in Sec. II, we introduce the simulation method used in this paper. In Sec. III-A, we present single electrical simulations starting with fitting the J-V curves obtained from experiment [13], [14], [21] to obtain material parameters of CZT, such as carrier lifetimes. In Sec. III-B, we present the double junction simulation, showing how can we reproduce most of unique features of the tandem cell behavior and identify the major sources of loss of the CZT/c-Si tandem cells. In Sec. III-C, we predict the efficiency of the ideal case, based on our model. In Sec. IV, we summarize our key findings.

II. Approach

In this paper, each simulation is performed using a semiconductor simulation tool known as Sentaurus Device [22], which solves for electrical and optical transport [23], [24] (shown in Fig. 3). The electrical simulation uses semiconductor transport equations coupled with Poisson's equation, while the optical simulation uses ray-tracing with the Beer-Lambert law to predict the light absorption in each layer. Although the emitter layer (n-CZT, n-Si) is very thin, the length of the primary absorption layers (p-CZT and p-Si) is significantly greater than the wavelength of incident light. So the Beer-Lambert law holds fairly accurate in this situation. In addition, because most of the layers are semiconductors, their refractive indices are very close (the refractive index of Si at the band edge is about 3.5, and for CZT it is about 3.2). So reflection between different layers can mostly be ignored. The reflection entering the structure is also assumed to be relatively low through the proper choice of refractive index and thickness for the antireflection coating. The parameters used in the simulation were obtained from experimental data or literature values [18]–[20], [25]. In addition, for tandem cells, the top and bottom cells are connected by a tunnel junction, where carrier transport is calculated quantum mechanically. Sentaurus provides a module which can simulate quantum mechanical inter-band tunneling using the WKB approximation. The tunnel junction simulation is coupled with the electrical drift-diffusion simulation and ray-tracing optics to obtain the simulation result in the tandem cell [22], [26], [27].

In these simulations, we treat all bulk carrier recombination as Shockley-Read-Hall (SRH) (i.e.. $\tau \approx \tau_{SRH}$), since it dominates the losses in this design. It has recently been shown that the radiative lifetime of CZT is $\tau_r \times n = 9.4 \times 10^9$ cm^{-3}·s [20], which is calculated by basic thermodynamic theory, where n is

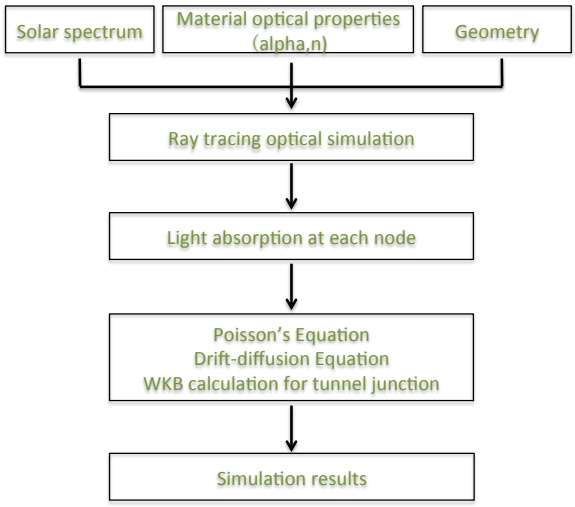

Fig. 3. The simulation process in Sentaurus Device for a given PV cell structure, which incorporates experimental data in an electro-optical simulation to calculate the J-V relation and efficiency, while quantifying the contributing loss mechanisms.

the density of majority carrier in cm^{-3}. At room temperature with $n = 10^{16}$ cm^{-3}, the SRH lifetime ($\tau_{SRH} = 55$ ns shown in TABLE I) is significantly longer than the radiative recombination time ($\tau_r = 940$ ns).

III. Results and Discussion

A. Single junction simulation

In this section, we present the unique aspects of our model for single junction CZT cells, and show the degree to which our model corresponds to experiment. In order to implement the approach outlined in the previous section, it is important to correctly estimate certain key values in the system. We begin by considering the doping profile of the CZT cell. In [21], n-type CZT is prepared by diffusing indium from the top surface. The doping density (dopant atoms density present in the crystal which is measured by SIMS analysis) is around 8×10^{20} cm^{-3} at the surface and decreases gradually to the junction, which can be described by the error function (the junction depth is set as 1.35 μm). However, not all dopants can be ionized at high doping. The effective n-type doping density (ionized density) is described by the formula [28]:

$$N_D^+ = \frac{N_D}{1 + g_D e^{(E_F + E_a - E_c)/kT}} \tag{1}$$

where $g_D = 2$ is the degeneracy factor, N_D is the doping density (dopant atoms density present in the crystal), E_F is the Fermi energy, E_c is the conduction band energy, and E_a is the activation energy.

The activation energy (E_a) for indium-doped CZT varies with bandgap and growth method [29], [30]. In this simulation, the activation energy is set to 0.16 eV [30], which yields a doping density near the surface of about 8×10^{17} cm^{-3}.

The highest measured lifetime value in experiment was 260 ns. However, doping can be higher in certain regions, which will decrease the mobility, and thus, the lifetime. Our

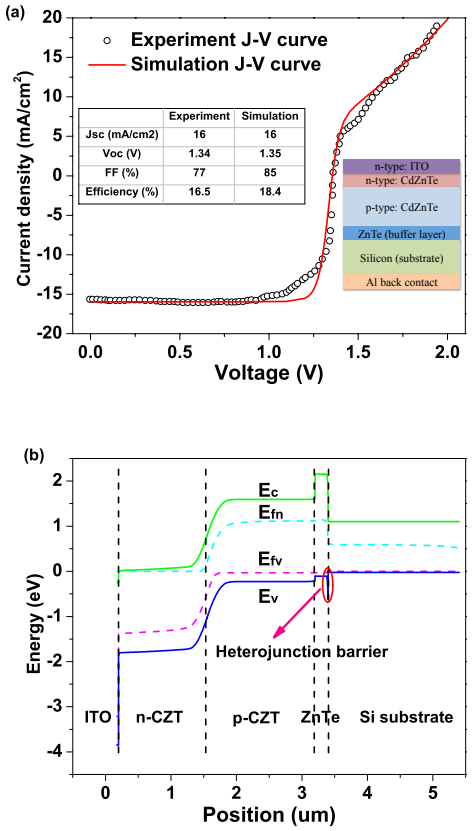

Fig. 4. (a) J-V analysis of a single junction CZT cell (E_g = 1.82 eV). The simulated J-V curve agrees well with the experimental J-V curve. However, the ideality factor near 1.2 V in the experiment curve is anomalously high ($\approx$ 5), which lowers the fill factor. The structure of single junction CZT is shown as an inset. (b) Energy band diagram of the single junction CZT cell under illumination with zero bias. The heterojunction barrier located between ZnTe and Si is generated by the difference of electron affinity values. This barrier causes rollover in the J-V curve, producing a linear region when current density goes beyond 5 mA/cm^2.

model for the bulk lifetime based on previous work is given by the formula [31]:

$$\tau = \tau_{min} + \frac{2(\tau_{max} - \tau_{min})}{1 + (N_D^+/N_{ref})^\gamma} \tag{2}$$

where N_{ref} = 1×10^{16} cm^{-3}, $\tau_{min} = 0$ ns, $\gamma = 1$ and τ_{max} is the lifetime at the reference doping.

We then fit the experimental J-V relation of the single junction CZT solar cell [13], [20], as shown in Fig. 4, by allowing τ_{max} to vary up to the highest measured lifetime value; an excellent match is achieved when $\tau_{max} = 55$ ns. In the experimental J-V curve, an anomalously high ideality factor is observed near 1.2 V, although the ideality factor rapidly decreases toward 1 at higher voltages. In [32] and [33], it is shown that dense grain boundary formation is a potential cause for this phenomenon. The heterojunction barrier that exists between ZnTe and silicon substrate shown in Fig. 4(b) can cause rollover in the J-V curve, resulting in a linear (resistor-like) I-V curve in the forward bias ($V > 1.4$ V) region when current density exceeds 5 mA/cm^2 [21], [34], [35]. This is proven by inspection of the band diagrams at

different applied voltages. When the voltage exceeds 1.4 V, most of the voltage drop occurs at the ZnTe/c-Si junction.

B. Double junction CZT/c-Si modeling and analysis of loss mechanisms

It is logical to employ the parameters obtained above (e.g. the lifetime of CZT) to model double-junction CZT/c-Si cells. However, if we do this without including any extra factors, the simulated CZT/c-Si J-V curve shown as a blue dashed line in Fig. 5(a) has a poor match to experiment (black circles). In the latter, two linear regions are observed: one at low voltage (region 1) and one at high voltage (region 2). The performance of the fabricated CZT/c-Si tandem cell is obviously worse than predicted. Thus, there must some other loss mechanism limiting the performance of the actual CZT/c-Si tandem cell.

In the presence of both series and shunt resistance, the J-V curve of the solar cell is given by:

$$J = J_0 e^{q(V-JR_s)/nkT} + \frac{V - JR_s}{R_{sh}} - J_L, \qquad (3)$$

where the J_L is the light generated current density (given approximately by $J_{sc} \times [1 + R_s/R_{sh}]$), J_0 is the dark saturation current density, V is the applied voltage, n is the ideality factor, R_{sh} is the shunt resistance and R_s is the series resistance. At low voltages, the current density changes proportionally to the shunt resistance, but at high voltages, the current density changes proportionally to the series resistance. Therefore, it is obvious that the linear curve in region 1 is caused by the shunt resistance, and the linear curve of region 2 is caused by the series resistance.

The experimental open circuit voltage of the CZT/c-Si tandem cell was 1.75 V [13], which is substantially lower than the combined V_{oc} of 2.01 V, calculated from adding each single junction cell: CZT with V_{oc} = 1.3 V (the bandgap of CZT used in the tandem cell is 1.78 eV, not 1.82 eV) [13] and c-Si with V_{oc} = 0.71 V [3]. At least three hypotheses could account for the deficit in open circuit voltage: the presence of a Schottky barrier, a poor tunnel junction or transport into anomalously p-doped shunting paths in the n-type CZT. The likelihood of each one is examined below.

Schottky Barrier: A non-Ohmic contact could result in a Schottky barrier at the back of Silicon and significantly decrease V_{oc} [21], [34], [35]. If the deficit of V_{oc} is caused by a Schottky barrier, the negative slope around 400 μm in the band diagram in Fig 5(c) shows that the Schottky barrier significantly limits the V_{oc} of CZT/c-Si tandem cells. After including shunt resistance, series resistance and a Schottky barrier, the simulated J-V curve shown as red solid curve in 5(a) is in very good agreement with experiment. The results are simulated by Sentaurus Device, which solves the drift-diffusion equation. The series resistance and shunt resistance are added afterwards. The baseline parameter values used in this work are provided in Table I.

Tunnel Junction: In Fig 5(c), the band structure of the tunnel junction is inset. The exact material used in the tunnel junction is unknown, but [21] states that this is a wide bandgap II-VI based tunnel junction. We choose p-ZnTe [19] and n-CdTe [18] for minimal series resistance, although CdTe is

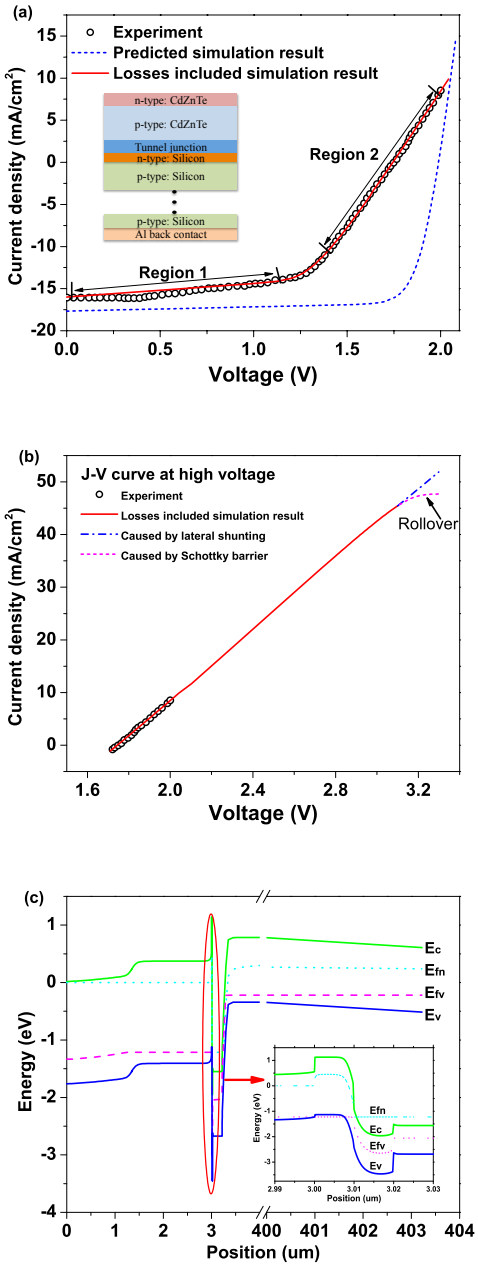

Fig. 5. (a) Experimental and two simulated J-V curves of the CZT/c-Si (E_g = 1.78/1.12 eV) tandem cell; its structure is inset. The dashed blue line shows the simulated J-V curve which does not include any extra losses from the single-junction case. The red solid line shows the simulated J-V curve which includes the shunt resistance, series resistance and Schottky barrier. In the experimental J-V curve, the shunt resistance ($\approx$ 600 Ω·cm^2) and the series resistance ($\approx$ 27 Ω·cm^2) are observed. An excellent correspondence between simulation and experiment is observed, with both deviating from the ideal diode equation. (b) J-V relation at high voltage. If the low V_{oc} is caused by a Schottky barrier, rollover into a flat region will occur around 3.2 V. Otherwise, current density will continue to increase with voltage. (c) Energy band diagram of the CZT/c-Si tandem cell under illumination with zero bias. The red circled region is the tunnel junction, which shows minimal series resistance. The negative slope of the energy band near the metal contacts, caused by the Schottky barrier, impedes carrier collection.

unlikely to be doped to such a high level in experiment, the use of CdTe as one tunnel junction material only lowers its impedance in the WKB quantum mechanical tunneling model in Sentaurus. The author does not provide details of the tunnel junction in the experiment [13], [20], but it is unlikely that the high series resistance comes from a poor tunnel junction. The classic tunnel junction current has a peak (shown in Fig. 6) [26] which is normally higher than the short circuit current under one sun of the solar cell. In addition, even if the tunnel current peak is lower than the J_{sc} of solar cell, the J-V curve of the solar cell will be changed and V_{oc} will be greatly decreased (shown in Fig. 7). Furthermore, the J-V curve will roll over at low voltages, contrary to the experimental observation reproduced in Fig. 5. Therefore, there is a negligible probability that the low efficiency of tandem CZT/c-Si cell is caused by the tunnel junction itself.

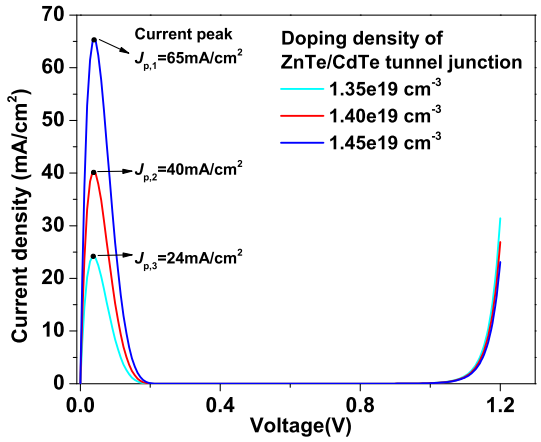

Fig. 6. Dark J-V curve for the ZnTe/CdTe tunnel junction only with different doping densities, as simulated by Sentaurus Device. The tunnel junction doping will significantly influence the current peak value; if it is lower than J_{sc}, the cell performance will be significantly decreased.

Through-thickness shunting path: If there are p-type shunting paths through the n-emitter (shown in the inset of Fig. 8), these shunting paths will limit the performance of CZT/Si tandem cell. This effect can be captured by a 2D simulation in Sentaurus Device. We assume there exists a p-type region within the n-emitter and simulate J-V curves by adjusting doping and width of this p-type region. The Fig. 8 shows the J-V curve of a single-junction CZT cell. From the figure, we find that the existence of the p-type region decreases the V_{oc}, and is related to the width of the p-type region. In addition, the p-type region will also cause shunt effects.

In the above discussion, we propose three hypotheses to explain the low V_{oc} in experiment. We find that a tunnel junction with excessively low peak current is the most unlikely reason for the low V_{oc}, which leaves the Schottky barrier and through-thickness shunting hypotheses. We can increase the applied voltage on the solar cell to help distinguish these two hypotheses. At high voltage, the Schottky barrier will impede the carrier transportation, inducing a rollover in the J-V curve, i.e. a flat region. However, if through-thickness shunting is the

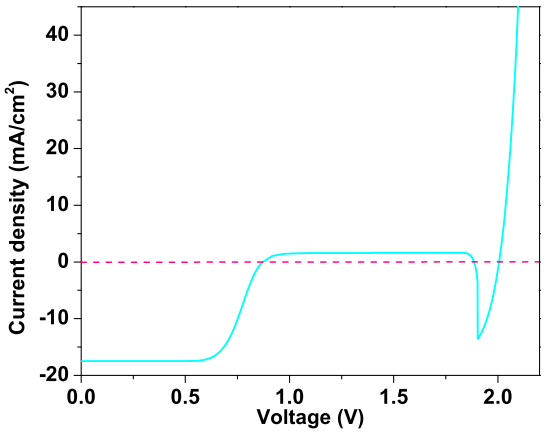

Fig. 7. Light J-V curve of CZT/c-Si tandem cell when the current peak of tunnel junction is lower than J_{sc}. The current peak is adjusted by doping density. Rollover of the J-V curve occurs at a much lower voltage (0.8 V) than observed in experiment (see Fig. 5).

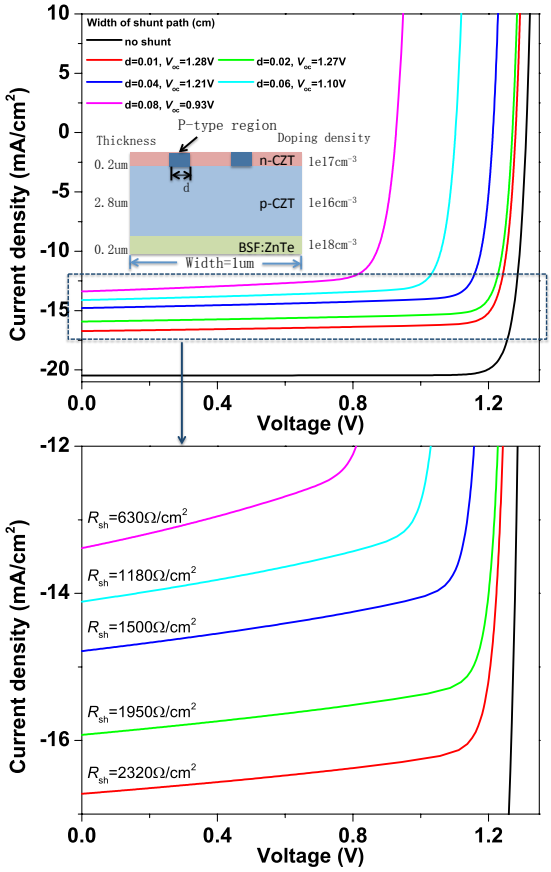

Fig. 8. The above figure shows the J-V curve as a function of the width of p-type region in n-emitter. The inset is the structure used in the simulation. We find V_{oc} decreases with increasing of shunt path width. The doping density of the p-type region is 1×10^{17}cm^{-3}. The figure below shows that shunt resistance decreases as the shunt path width increases.

cause for low V_{oc}, there will not be rollover in the high-voltage region of the J-V curve. Instead, the current will continue to increase as a function of voltage. Both predictions are shown in Fig. 5(b). It is evident that the two curves will only diverge at forward biases of 3.2 V or higher. This result explains why neither hypothesis can be ruled out based on existing experimental data, which only extends to a forward bias of 2 V.

TABLE I
DEVICE PARAMETERS FOR (A) BASELINE TOP CELL, (B) BASELINE TUNNEL JUNCTION, (C) BASELINE BOTTOM CELL AND (D) GLOBAL PARAMETERS

(a) Top cell		n-CZT/p-CZT [18], [20]	
E_g (eV)	1.78	$N_{D/A}$ (cm^{-3})	D(x)*/1×10^{16}
W (μm)	1.35/1.65	$\tau_{SRH}(ns)$	τ(x)*,†/55†
N_C (cm^{-3})	8×10^{17}	N_V (cm^{-3})	1.8×10^{19}
μ_e (cm^2/V-s)	1500	μ_h (cm^2/V-s)	100
Electron affinity (eV)		4.1	

(b) Tunnel junction		p-ZnTe [19]/n-CdTe [18]	
E_g (eV)	2.26/1.5	$N_{D/A}$ (cm^{-3})	1×10^{20}‡
W(μm)	0.01‡/0.01‡	$\tau_{SRH}(ns)$	0.1‡
Electron affinity (eV)		3.53/4.4	

(c) Bottom cell		n-Si [25]/p-Si [20], [25]	
E_g (eV)	1.12	$N_{D/A}$ (cm^{-3})	10^{20}‡/10^{17}
W(μm)	0.2‡/400†	$\tau_{SRH}(ns)$	1‡/10^5†
$C_{n,Auger}$ (cm^6/s)	1.1×10^{-30}	$C_{p,Auger}$ (cm^6/s)	0.3×10^{-30}
N_C (cm^{-3})	2.8×10^{19}	N_V (cm^{-3})	1.04×10^{19}
μ_e (cm^2/V-s)	1.4/1400	μ_h (cm^2/V-s)	0.4/400
Electron affinity (eV)		4.05	

(d) Global parameters	
$\Phi_{bp} = E_f - E_V$ (eV)	0.51†
Series Resistance (Ω/cm^2)	27†
Shunt Resistance (Ω/cm^2)	600†

* highly dependent on position in device
† parameter value obtained from fitting experimental J-V curve
‡ parameter is set to a reasonable value for tandem cell

C. Modeling improvements

In order to explore the potential efficiency of the CZT/c-Si tandem cell, we start from the baseline of the experiment, and remove each loss mechanism one-by-one. If the low V_{oc} is caused by the Schottky barrier formed at the back contact, one may add another material nearby to form a back surface field, or change the back contact material itself [36]. As shown in Fig. 9, once the Schottky barrier is eliminated, the tandem V_{oc} increases from 1.75 V to 1.98 V. Then, in the absence of the Schottky barrier, we gradually adjust the series and shunt resistances. The high series resistance measured in the experiment could be caused by a non-Ohmic contact between the n-type CZT and the metal grid. However, properly

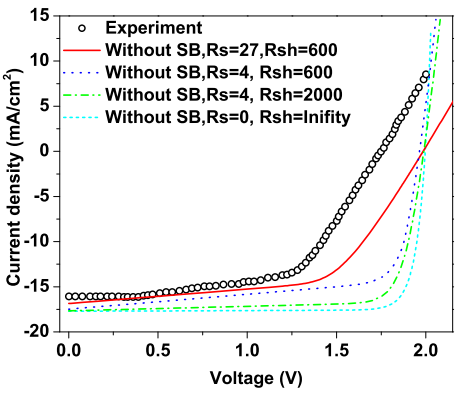

Fig. 9. J-V curves of CZT/c-Si tandem cells. Mitigating three key sources of losses gradually increases cell efficiency from 17% to 30.6%. The unit for R_s and R_{sh} in the figure is Ω·cm^2.

depositing an indium layer on top of n-type CZT should lower series resistance to 4 Ω· cm^2 [21]. In addition, for the tandem CZT/c-Si cell, the top CZT cell may be deposited on a different material which will cause large lattice mismatch and defects, which may behave like grain boundaries. The existence of defects (e.g., stacking faults [37]) or grain boundaries inside CZT will provide shunt paths for current flow through the top cell. Therefore, the diffusion of metal and grain boundaries inside CZT cell can potentially vary the shunt resistance (600—2000 Ω· cm^2 under illumination). [38]–[41]. Increasing the grain size of CZT and applying appropriate $CdCl_2$ treatment [42] during fabrication may increase the shunt resistance to a more reasonable value. If series resistance can be decreased to 4 Ω· cm^2, shunt resistance can be increased to 2000 Ω· cm^2. As a result, J_{sc} increases to 17.7 mA/cm^2 and the fill factor increases to 79.8%, with only a slight change in V_{oc}, resulting in an efficiency of 28.1%. If all the loss mechanisms can be completely eliminated, then the efficiency of CZT/c-Si tandem cells could be improved to 30.6%; however, 28.1% is a much more experimentally feasible value (shown in TABLE II).

As mentioned previously, the low V_{oc} can also be induced by shunting paths inside n-emitter. Pinpointing the origin of the shunts may require further investigation. The presence of shunting in tandem cell is a known problem in other types of tandem cells [43]–[45], and judging from the reported performance of fabricated CZT/Si tandem cell, it likely suffers from the same problem. In addition, this hypothesis can be tested and verified through using EBIC investigation [39]. If this through-thickness shunting, together with series resistance and other shunt effect, is reduced to the minimum feasible level, the efficiency of CZT/c-Si tandem cell can be increased to 30.6%; however, 28.1% is a much more experimentally feasible value, as shown in TABLE II.

Besides the loss mechanisms mentioned above, the non-ideal doping profile of top CZT cell and leakage current in the bottom Si cell also both limit the efficiency. It is shown that the experimental thickness of n-type CZT in the tandem cell (1.35 μm) is far from the ideal thickness of a few hundred

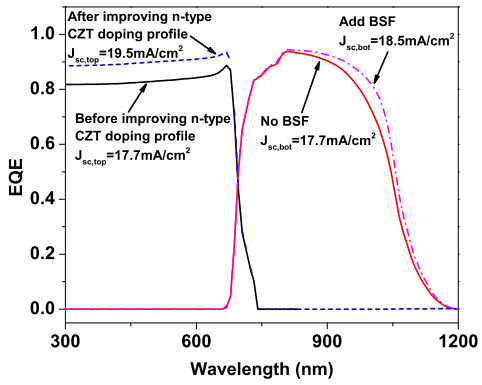

Fig. 10. Simulated external quantum efficiency of the CZT/c-Si tandem cell. An improved doping profile increases the J_{sc} in the CZT layer up to 18.8 mA/cm^2, and adding a BSF increases J_{sc} in the silicon layer up to 18.5 mA/cm^2.

nanometers, and that its doping density near the top surface is too high (8×10^{17}cm^{-3}) [21], which decreases carrier lifetimes and increases bulk recombination [46]. In the experiment, the n-type CZT was doped by high temperature indium diffusion annealing, which extends the doped region beyond the optimum. Thus, one may choose iodine doping to improve the doping profile [47]. Applying a thinner n-type CZT layer with a modest doping of 10^{17} cm^{-3} enhances photo-generated current in the CZT layer up to 18.8 mA/cm^2, as shown in Fig. 10. In addition, the recombination at contact can be reduced by adding a highly-doped thin layer, known as a back surface field (BSF), near the back contact. In Fig. 10, the BSF increases the J_{sc} of the silicon layer up to 18.5 mA/cm^2. Table II provides the V_{oc}, J_{sc}, fill factor and efficiency for the experiment [13] and our simulation results. When all intrinsic loss mechanisms are adjusted to reasonable values, extrinsic losses are eliminated, and the suggested designs are applied, the highest achievable efficiency is predicted as 32.6%. The same result also holds for the alternative through-thickness shunting hypothesis.

TABLE II
PREDICTED EFFICIENCIES OF CZT/C-SI TANDEM CELL REGARDING THREE LIMITING FACTORS. SB, R_S AND R_{SH} INDICATE SCHOTTKY BARRIER, SERIES RESISTANCE AND SHUNT RESISTANCE, RESPECTIVELY.

	V_{oc} (V)	J_{sc} (mA/cm^2)	FF (%)	η (%)
Experiment [13]	1.75	16	60	16.8
Simulation	1.75	16.0	59.5	16.7
No SB	1.98	16.9	59.8	20.0
No SB, R_s=4	1.96	17.5	71.4	24.5
No SB, R_s=4, R_s=2000	1.99	17.7	79.8	28.1
No SB, R_s=0, R_s=Infinity	2.00	17.7	86.6	30.6
Improved doping profile and BSF	2.01	18.5	88.0	32.6

The highest possible efficiency of the CZT/c-Si tandem cell is 32.6% when the bandgap of CZT is 1.78 eV. Based on our model, we can predict the highest efficiency of CZT/c-Si tandem cells by varying the bandgap of CZT while holding all other material parameters fixed. The efficiency of CZT/c-Si tandem cell for different bandgap is shown in Fig. 11. The highest efficiency is 34.1% when E_g=1.8 eV and at this bandgap, V_{oc}=2.02 V, J_{sc}=19.2 mA. Finally, breakthroughs in material deposition quality could lead to much higher performance, potentially even approaching the 45% theoretical limit.

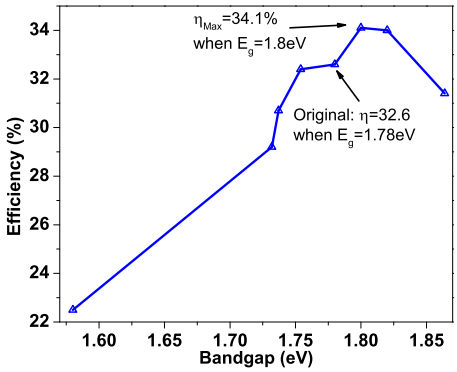

Fig. 11. The efficiency of CZT/c-Si tandem cell for different CZT bandgap. The highest efficiency is 34.7% when the bandgap is equal to 1.8 eV.

IV. CONCLUSION

We investigated a tandem cell structure utilizing II-IV cadmium-zinc telluride alloys and silicon substrates, which theoretically can have 45% cell efficiency with one sun illumination. In the CZT/c-Si stacked configuration, we successfully reproduced experimental observations using our simulation framework for both single-junction crystalline CZT (η =16%) and tandem CZT/c-Si (η =16.8%). By studying the loss mechanisms of the CZT/c-Si cell, we confirmed that while shunt and series resistance are two limiting factors in the design of CZT/c-Si tandem cells, a third mechanism also plays a key role in decreasing V_{oc}. We propose three hypotheses to explain these observations: a poor tunnel junction, a Schottky barrier or through-thickness shunting. Among them, the hypothesis that the low V_{oc} is caused by poor tunnel junction with a low peak current is the most unlikely and can be eliminated. We also proposed that measuring the J-V curve at high voltage can unambiguously distinguish the remaining two hypotheses. The fourth and final source of loss is current mismatch, induced by a non-ideal doping profile and lack of a back surface field, which may also lower the efficiency. Through physics-based modeling, we propose four strategies to mitigate these loss mechanisms. First, an indium-based contact for CZT can significantly lower the series resistance. Second, increasing the effective CZT grain size and applying appropriate $CdCl_2$ treatment during fabrication can help lower shunt resistance. Third, if higher-voltage measurements demonstrate the presence of a Schottky barrier, then a suitable BSF material should be chosen to lower

it to help the carrier collection. Fourth, using iodine instead of indium as a dopant can help bring the junction depth up to where the most absorption and carrier generation takes place. Making these modifications can boost the efficiency up to 32.6%. Furthermore, if a slightly different alloy of CZT with a bandgap $E_g = 1.8$ eV can be grown, current mismatch can be mostly eliminated, thus raising the efficiency even further, up to 34.1%. The world-record efficiency of tandem cell is 31.1% (InGaP/GaAs tandem cell [48]), which is made using a MOPVE growth process without epitaxial lift-off [48]. It has been predicted in simulation that the efficiency of this type of cell can achieve up to 34.5% [49] in simulation. Compared to the InGaP/GaAs tandem cell, CZT/Si tandem cell has greater potential for improvement, since the experimental efficiency (16.8%) is much lower than our predicted value (34.1%). In addition, the fabrication cost of CZT/c-Si tandem cell could be much lower.

REFERENCES

[1] Panasonic, Available: http: //panasonic.co.jp/corp/news/official.data/data.dir/2014/04/en140410-4/en140410-4.html, Accessed on: Oct. 30, 2014.

[2] First Solar, Available: http://investor.firstsolar.com/releases.cfm?sect=all, Accessed on: Oct. 30, 2014.

[3] M. A. Green, K. Emery, Y. Hishikawa, W. Warta, and E. D. Dunlop, "Solar cell efficiency tables (version 44)," *Prog. Photovolt.: Res. Appl.*, vol. 22, pp. 701–710, 2014.

[4] A. Goodrich, T. James, and M. Woodhouse, "Residential, commercial, and utilityscale photovoltaic (PV) system prices in the united states: current drivers and cost-reduction opportunities," *Contract*, vol. 303, pp. 275–3000, 2012.

[5] Greentechmedia, Available: http: //www.greentechmedia.com/articles/read/us-solar-carport-market-poised-for-record-year-continued-growth, Accessed on: Oct 30, 2014.

[6] W. Shockley and H. J. Queisser, "Detailed balance limit of efficiency of p-n junction solar cells," *J. Appl. Phys.*, vol. 32, no. 3, pp. 510–519, 1961.

[7] L. Kazmerski, "Research and device problems in photovoltaics," *Solar Materials Science*, vol. 1, pp. 551–584, 1980.

[8] A. Imenes and D. Mills, "Spectral beam splitting technology for increased conversion efficiency in solar concentrating systems: a review," *Sol. Energy Mater. Sol. Cells*, vol. 84, no. 1, pp. 19–69, 2004.

[9] A. Polman and H. A. Atwater, "Photonic design principles for ultrahigh-efficiency photovoltaics," *Nat. Mater*, vol. 11, no. 3, pp. 174–177, 2012.

[10] M. A. Green, "Third generation photovoltaics: Ultra-high conversion efficiency at low cost," *Prog. Photovolt.: Res. Appl.*, vol. 9, no. 2, pp. 123–135, 2001.

[11] C. H. Henry, "Limiting efficiencies of ideal single and multiple energy gap terrestrial solar cells," *J. Appl. Phys.*, vol. 51, no. 8, pp. 4494–4500, 1980.

[12] D. Staebler and C. Wronski, "Reversible conductivity changes in discharge-produced amorphous Si," *Appl. Phys. Lett.*, vol. 31, no. 4, pp. 292–294, 1977.

[13] M. Carmody, S. Mallick, J. Margetis, R. Kodama, T. Biegala, D. Xu, P. Bechmann, J. Garland, and S. Sivananthan, "Single-crystal II-VI on Si single-junction and tandem solar cells," *Appl. Phys. Lett.*, vol. 96, no. 15, p. 153502, 2010.

[14] D. Xu, T. Biegala, M. Carmody, J. W. Garland, C. Grein, and S. Sivananthan, "Proposed monolithic triple-junction solar cell structures with the potential for ultrahigh efficiencies using II–VI alloys and silicon substrates," *Appl. Phys. Lett.*, vol. 96, no. 7, p. 073508, 2010.

[15] P. M. Tribolet, P. Chorier, A. Manissadjian, P. Costa, and J.-P. Chatard, "High-performance infrared detectors at sofradir," in *AeroSense 2000*. International Society for Optics and Photonics, 2000, pp. 438–456.

[16] A. Rogalski, "HgCdTe infrared detector material: history, status and outlook," *Rep. Prog. Phys.*, vol. 68, no. 10, p. 2267, 2005.

[17] M. J. DiNezza, X.-H. Zhao, S. Liu, A. P. Kirk, and Y.-H. Zhang, "Growth, steady-state, and time-resolved photoluminescence study of CdTe/MgCdTe double heterostructures on InSb substrates using molecular beam epitaxy," *Appl. Phys. Lett.*, vol. 103, no. 19, p. 193901, 2013.

[18] M. Gloeckler, A. Fahrenbruch, and J. Sites, "Numerical modeling of CIGS and CdTe solar cells: setting the baseline," in *Photovoltaic Energy Conversion, 2003. Proc. of 3rd World Conf. on*, vol. 1. IEEE, 2003, pp. 491–494.

[19] K. Sato and S. Adachi, "Optical properties of ZnTe," *J. Appl. Phys.*, vol. 73, no. 2, pp. 926–931, 1993.

[20] J. Garland, T. Biegala, M. Carmody, C. Gilmore, and S. Sivananthan, "Next-generation multijunction solar cells: The promise of II-VI materials," *J. Appl. Phys.*, vol. 109, no. 10, p. 102423, 2011.

[21] M. Carmody and A. Gilmore, "High efficiency single crystal CdTe solar cells," *NREL Report*, 2011.

[22] T. Synopsys, "Sentaurus. synopsys," *Inc., c-2009.06 ed*, 2009.

[23] D. Vasileska and S. Goodnick, "Computational electronics," *Synthesis Lectures on Computational Electromagnetics*, vol. 1, no. 1, pp. 1–216, 2005.

[24] S. Selberherr, *Analysis and simulation of semiconductor devices*. New York, NY, USA: Springer Wien, 1984.

[25] J. Singh, *Physics of Semiconductors and their Heterostructures*. New York, NY, USA: McGraw-Hill, 1993, vol. 64.

[26] M. Hermle, G. Letay, S. Philipps, and A. W. Bett, "Numerical simulation of tunnel diodes for multi-junction solar cells," *Prog. Photovolt.: Res. Appl.*, vol. 16, no. 5, pp. 409–418, 2008.

[27] M. Ieong, P. M. Solomon, S. Laux, H.-S. Wong, and D. Chidambarrao, "Comparison of raised and schottky source/drain mosfets using a novel tunneling contact model," in *Electron Devices Meeting, 1998. IEDM'98. Technical Digest., International*. IEEE, 1998, pp. 733–736.

[28] R. F. Pierret and G. W. Neudeck, *Advanced semiconductor fundamentals*. Boston, MA, USA: Addison-Wesley Reading, 1987, vol. 6.

[29] T. Wang, W. Jie, D. Zeng, G. Yang, Y. Xu, W. Liu, and J. Zhang, "Temperature dependence of photoluminescence properties of In-doped cadmium zinc telluride," *J. Mater. Res.*, vol. 23, no. 05, pp. 1389–1392, 2008.

[30] G. Yang, W. Jie, Q. Li, T. Wang, G. Li, and H. Hua, "Effects of In doping on the properties of CdZnTe single crystals," *J. Cryst. Growth*, vol. 283, no. 3, pp. 431–437, 2005.

[31] J. Fossum, R. Mertens, D. Lee, and J. Nijs, "Carrier recombination and lifetime in highly doped silicon," *Solid-State Electron.*, vol. 26, no. 6, pp. 569–576, 1983.

[32] J. D. Major, Y. Y. Proskuryakov, and K. Durose, "Nucleation and grain boundaries in thin film CdTe/CdS solar cells," in *MRS Proc.*, vol. 1165. Cambridge Univ Press, 2009, pp. 1165–M06.

[33] E. S. Mungan, Y. Wang, S. Dongaonkar, D. R. Ely, R. E. Garcia, and M. A. Alam, "From process to modules: end-to-end modeling of CSS-deposited CdTe solar cells," *IEEE J. Photovolt.*, vol. 4, no. 3, pp. 954–961, 2014.

[34] A. Niemegeers and M. Burgelman, "Effects of the Au/CdTe back contact on IV and CV characteristics of Au/CdTe/CdS/TCO solar cells," *J. Appl. Phys.*, vol. 81, no. 6, pp. 2881–2886, 1997.

[35] M. Köntges, R. Reineke-Koch, P. Nollet, J. Beier, R. Schäffler, and J. Parisi, "Light induced changes in the electrical behavior of CdTe and Cu(In, Ga)Se_2 solar cells," *Thin Solid Films*, vol. 403, pp. 280–286, 2002.

[36] A. Yu, "Electron tunneling and contact resistance of metal-silicon contact barriers," *Solid-State Electron.*, vol. 13, no. 2, pp. 239–247, 1970.

[37] S.-H. Yoo, K. T. Butler, A. Soon, A. Abbas, J. M. Walls, and A. Walsh, "Identification of critical stacking faults in thin-film CdTe solar cells," *Appl. Phys. Lett.*, vol. 105, no. 6, p. 062104, 2014.

[38] M. Gloeckler, J. R. Sites, and W. K. Metzger, "Grain-boundary recombination in Cu(In, Ga)Se_2 solar cells," *J. Appl. Phys.*, vol. 98, no. 11, p. 113704, 2005.

[39] O. Breitenstein, J. Rakotoniaina, M. H. Al Rifai, and M. Werner, "Shunt types in crystalline silicon solar cells," *Prog. Photovolt.: Res. Appl.*, vol. 12, pp. 529–538, 2004.

[40] S. Dongaonkar, J. D. Servaites, G. M. Ford, S. Loser, J. Moore, R. M. Gelfand, H. Mohseni, H. W. Hillhouse, R. Agrawal, M. A. Ratner *et al.*, "Universality of non-Ohmic shunt leakage in thin-film solar cells," *J. Appl. Phys.*, vol. 108, no. 12, p. 124509, 2010.

[41] S. Dongaonkar, Y. Karthik, D. Wang, M. Frei, S. Mahapatra, and M. A. Alam, "On the nature of shunt leakage in amorphous silicon pin solar cells," *IEEE Electron Device Lett.*, vol. 31, no. 11, pp. 1266–1268, 2010.

[42] T. Razykov, N. Amin, B. Ergashev, C. Ferekides, D. Goswami, M. Hakkulov, K. Kouchkarov, K. Sopian, M. Sulaiman, M. Alghoul *et al.*, "Effect of $CdCl_2$ treatment on physical properties of CdTe films with different compositions fabricated by chemical molecular beam deposition," *Applied Solar Energy*, vol. 49, no. 1, pp. 35–39, 2013.

[43] J. Y. Kim, K. Lee, N. E. Coates, D. Moses, T.-Q. Nguyen, M. Dante, and A. J. Heeger, "Efficient tandem polymer solar cells fabricated by all-solution processing," *Science*, vol. 317, no. 5835, pp. 222–225, 2007.
[44] M. Afzaal and P. O'Brien, "Recent developments in II–VI and III–VI semiconductors and their applications in solar cells," *Journal of Materials Chemistry*, vol. 16, no. 17, pp. 1597–1602, 2006.
[45] P. Mahawela, G. Sivaraman, S. Jeedigunta, J. Gaduputi, M. Ramalingam, S. Subramanian, S. Vakkalanka, C. Ferekides, and D. Morel, "II–VI compounds as the top absorbers in tandem solar cell structures," *Materials Science and Engineering: B*, vol. 116, no. 3, pp. 283–291, 2005.
[46] M. Lundstrom, *Fundamentals of carrier transport*. New York, NY, USA: Cambridge University Press, 2009.
[47] D. Rajavel and C. Summers, "Gas source iodine n-type doping of molecular beam epitaxially grown CdTe," *Appl. Phys. Lett.*, vol. 60, no. 18, pp. 2231–2233, 1992.
[48] M. Steiner, J. F. Geisz, I. Garcia, D. J. Friedman, A. Duda, W. J. Olavarria, M. Young, D. Kuciauskas, and S. R. Kurtz, "Effects of internal luminescence and internal optics on V_{oc} and J_{sc} of III–V solar cells," *IEEE J. Photovolt.*, vol. 3, no. 4, pp. 1437–1442, 2013.
[49] P. Nayak, J. Dutta, and G. Mishra, "Efficient InGaP/GaAs DJ solar cell with double back surface field layer," *Engineering Science and Technology, an International Journal*, 2015.